13

High-Pressure Na-Ca Carbonates in the Deep Carbon Cycle

Sergey Rashchenko[1,2], Anton Shatskiy[1,2,3], and Konstantin Litasov[1,2,3]

ABSTRACT

Carbonates play a central role in the subduction transport of oxidized carbon from Earth's surface to the deep mantle. The melting of carbonated rocks also leads to the release of carbonate melts, regarded as important oxidizing and metasomatizing agents, from the subducting slab. Although at upper mantle conditions the chemistry of carbonates within the subducting slab is restricted to the thoroughly studied ternary $CaCO_3$-$MgCO_3$-$FeCO_3$ system, recent experimental and natural evidences strongly suggest that at conditions of the mantle transition zone, Na-Ca carbonates become the main host of oxidized carbon and define solidus temperatures and chemistry of deep melts. In this chapter, we discuss transport of carbonates to the mantle transition zone within the subducting slab, evidences of sodium migration from silicates into carbonates under high pressure, and crystal chemistry of currently known high-pressure Na-Ca carbonates.

13.1. CARBONATES IN SUBDUCTION INFLUX OF CARBON

Although deep reservoirs can host carbon in both reduced (diamond, carbides, reduced C-O-H fluid) and oxidized (carbonates, CO_2) forms, the transport of carbon from Earth's surface to mantle depths is indeed dominated by its oxidized form: carbonates.

According to data from the Ocean Drilling Program (ODP), the most carbon-rich part of the subducting lithosphere is its sedimentary layer, which hosts 2–3 wt.% of CO_2, predominantly in the form of carbonates (Plank & Langmuir, 1998; Staudigel, 2014). The latter corresponds to the subduction influx of 8.9×10^{11} mol C/year. Hydrothermal alteration also leads to the accumulation of carbon in basaltic oceanic crusts, up to the average CO_2 content established by the ocean drilling program of 0.2 wt.% (Shilobreeva et al., 2011). Of these, ~80% correspond to carbonates, while the remaining 20% represent hydrocarbons and other organic carbon species. The smaller CO_2 content compared to overlying sedimentary layer is compensated by the ~7 km thickness of basaltic oceanic crust, which provides a carbon flux of 2.9×10^{12} mol C/year (i.e. more than three times higher than that from sediments).

The most controversial reservoir of subducting carbon is serpentinized peridotites localized in the lower part of the oceanic lithosphere. The results of ODP demonstrate that significant amounts of carbonates may appear during hydrothermal serpentinization of peridotite, so that up to 13 vol.% of the resulting serpentinite may be represented by carbonate veins (Kodolányi et al., 2011). An estimated degree of serpentinization of lithospheric peridotites entering the subduction zone, however, varies from ~10% in models considering bending faults-related serpentinization (Faccenda, 2014) to the order of magnitude lower in models that reject the latter phenomenon (Korenaga, 2017). An average carbonate content of related serpentinites also remains unclear. Moreover, a well-known process of CO_2 and carbonate reduction into abiogenic methane and graphite during serpentinization of peridotite (Brovarone et al., 2017, and references therein) raises additional question about the abundance

[1] *Sobolev Institute of Geology and Mineralogy, Novosibirsk, Russia*

[2] *Novosibirsk State University, Novosibirsk, Russia*

[3] *Vereshchagin Institute for High Pressure Physics, Moscow, Russia*

Carbon in Earth's Interior, Geophysical Monograph 249, First Edition. Edited by Craig E. Manning, Jung-Fu Lin, and Wendy L. Mao.

of carbonates in serpentinized peridotites. On the other hand, Debret et al. (2015) recently pointed out that inevitable deserpentinization of subducted peridotites enriched in Fe^{3+}, will lead to the release of oxidizing fluids (between FMQ + 1 and FMQ + 4), definitely incompatible with any hosts of reduced carbon in the subducting slab.

Even if abiogenic methane from the serpentinized peridotites and organic compounds from the overlying basaltic oceanic crust and sedimentary layer represent a significant part of subduction carbon influx, they readily leave the slab during devolatilization. In contrast, stabilization of aragonite, dolomite, and magnesite inhibits the carbon escape (Kerrick & Connolly, 2001; Litasov, 2011), making carbonates the main reservoir transporting carbon from Earth's surface to mantle depth.

13.2. SUBDUCTED CARBONATES IN THE UPPER MANTLE

The mineralogy of carbonates entering subduction zones within subducting slabs is represented by calcite, biogenic aragonite, dolomite, magnesite (occurring in serpentinites), and sedimentary Mg-calcite, often with admixture of Fe^{2+}. During subduction-related high-pressure metamorphism, calcite transforms into aragonite, and dolomite decomposes into aragonite + magnesite (Luth, 2001; Sato & Katsura, 2001), so the latter two become the main carbon reservoir in the slab sinking through the upper mantle. The fate of carbon in the slab depends on the position of subduction geotherm in relation to the solidus of carbonated pelite (for carbonates delivered within sedimentary layer) or eclogite (for those from basaltic oceanic crust).

The exact composition of subducting eclogite and pelite, however, is poorly constrained, and a range of solidi is reported for corresponding systems depending on composition and H_2O content (see reviews: Hammouda & Keshav, 2015; Litasov & Shatskiy, 2018; Stagno, 2019, and references therein). According to Grassi and Schmidt (2011), warm subduction geotherms cross the solidus of carbonated pelite between 6 and 9 GPa depending on H_2O content (~190–270 km), where decarbonation melting produces potassium-rich carbonate melts (Table 13.1). In the case of colder geotherms (especially in dry conditions), aragonite and magnesite can escape melting, being transported further to the mantle transition zone (Grassi & Schmidt, 2011). The solidus of carbonated eclogite is a few hundred degrees higher, so the hot subduction geotherm crosses it only near 13 GPa (~390 km) with production of calcium-rich carbonate melts (Table 13.1), whereas average and cold geotherms allow the transport of magnesite directly to the mantle transition zone (Thomson et al., 2016).

13.3. SUBDUCTED CARBONATES IN THE MANTLE TRANSITION ZONE

As we mentioned above, subducted carbonates in the form of aragonite and magnesite can be transported to the mantle transition zone within carbonated pelites along the cold subduction geotherm, and within carbonated eclogites along average and cold ones. The latter agrees with the data of Kiseeva et al. (2018), who observed an anomalous Fe^{3+} enrichment in garnets originated from the mantle transition zone, and suggested that corresponding oxidizing agents are carbonates delivered to the mantle transition zone by subduction. The oxidizing nature of subducted carbonates results from the fact that carbonate ↔ carbon equilibria buffer oxygen fugacity several log units higher than typical for deep mantle values close to iron ↔ wustite buffer (Stagno, 2019; Stagno et al., 2015).

Although $CaCO_3$ and $MgCO_3$ polymorphs stable at lower mantle pressures were extensively studied in the last decade (Gavryushkin et al., 2017; Merlini et al., 2017; Oganov et al., 2008; Pickard & Needs, 2015; etc.), a widespread treatment of such phases as lower mantle carbon hosts should be justified by investigation of whether the transport of carbonates to the lower mantle via mantle transition zone is possible in real lithologies. Related data were reported by Grassi and Schmidt (2011) for carbonated pelite, Litasov et al. (2013) for alkali-bearing carbonatite compositions, and Thomson et al. (2016) for carbonated eclogite, who observed two important phenomena: (1) at pressures of the mantle transition zone, the solidus of carbonated rocks dramatically drops over a narrow pressure interval by 100–200 °C, and (2) at the same pressures, new Na-Ca-carbonate substitute aragonite and magnesite in the subsolidus assemblage.

According to Grassi and Schmidt (2011), carbonated pelite, delivered to the mantle transition zone along colder subduction geotherms, will melt near 20 GPa (~570 km) during the heating of deflected slab towards mantle adiabat. The resulting carbonatite melt, however, drastically differs from that produced during the melting of carbonated pelite along warm subduction geotherms in the upper mantle (Table 13.1). Whereas potassium behaves as an incompatible element during melting at upper mantle pressures, giving 24 wt.% K_2O in the K-Ca carbonate melt, it completely switches behavior in the mantle transition zone, so that corresponding carbonate melt possesses 3 wt.% of K_2O and is not significantly enriched in potassium compared with the bulk rock (Table 13.1). In contrast, sodium, being perfectly compatible during melting at upper mantle pressure (just 1 wt.% Na_2O in the melt, Table 13.1), becomes highly incompatible as soon as melting occurs in the mantle transition zone, so that the Na_2O content of the corresponding Na-Ca carbonate melt reaches 23 wt.%. (Table 13.1). A similar phenomenon

Table 13.1 Compositions of near-solidus carbonate melts derived from dry carbonated pelite (Grassi & Schmidt, 2011) and eclogite (Thomson et al., 2016) in the upper mantle (UM) and mantle transition zone (MTZ), and subsolidus Na-Ca-carbonates stable in the MTZ.

	Carbonated Pelite				Carbonated Eclogite			
	Starting Material	UM Melt	MTZ Melt	Subsolidus Carbonate*	Starting Material	UM Melt	MTZ Melt	Subsolidus Carbonate*
wt. %		8 GPa 1100 °C	22 GPa 1500 °C	22 GPa 1400 °C		13.1 GPa 1450 °C	20.7 GPa 1200 °C	20.7 GPa 1100 °C
CO_2	4.5	43.67	43.12	41.91	2.52	41.88	45.78	43.55
SiO_2	54.63	0.26	0.05	–	50.35	0.36	1.10	–
CaO	5.88	16.3	15.3	34.84	10.80	33.61	26.03	38.39
MgO	2.92	2.95	7.36	5.72	7.15	6.67	6.66	3.54
FeO	4.86	7.55	7.32	6.15	11.35	9.50	8.25	1.61
Na_2O	3.20	0.95	22.7	11.04	2.48	4.63	10.04	12.10
K_2O	2.21	24.4	3.27	0.33	0.06	0.76	0.39	0.56
CaO/Na_2O	1.84	17.16	0.67	3.16	4.35	7.26	2.59	3.17
K_2O/Na_2O	0.69	25.68	0.14	0.03	0.02	0.16	0.04	0.05

* Coexisting with magnesite.

was reported by Thomson et al. (2016) for carbonated eclogite that also melts near 20 GPa (~570 km) being subducted along an average subduction geotherm: the Na_2O content of the mantle transition zone Ca-Na carbonate melt (10 wt.%) is twice than that of the melt produced in the upper mantle.

The reason for the change in alkali speciation is the appearance of a new Na-Ca carbonate mineral that is stable in the subsolidus assemblages (Table 13.1), which (1) effectively extracts Na_2O from silicates into fusible carbonate phase, (2) drastically lowers the solidus temperatures, and (3) provides specific Ca-Na carbonate melts when the solidus is crossed by a geotherm. The idealized formula of this Na-Ca carbonate is $(Na,K)_2(Ca,Mg,Fe)_4(CO_3)_5$, with pronounced dominance of Na and Ca cations (Table 13.1). The recent findings of Na-Ca carbonates in inclusions in "superdeep" Juina diamonds (Kaminsky, 2017) that allowed to distinguish "deep natrocarbonatite association" strongly support the experimental data on the existence of Na-Ca-carbonate and related melts in the mantle transition zone.

The reported Na-Ca carbonate formation is closely related to the strong enrichment of subducting pyroxene in $NaAlSi_2O_6$ end-member due to preferential dissolution of sodium-poor end-members into coexisting majoritic garnet, so that above 13 GPa, pyroxene in both carbonated pelite and eclogite is represented by nearly pure jadeite (Grassi & Schmidt, 2011; Thomson et al., 2016). In carbonate-free lithologies, the further pressure increase would lead to the dissolution of jadeite in majoritic garnet in the form of Na-majorite end-member. In contrast, in carbonated lithologies above 13 GPa (~390 km), jadeite reacts with Ca-Mg carbonates, producing Na-Ca carbonate.

The corresponding reaction in carbonated pelite takes place between 13 and 16 GPa (Grassi & Schmidt, 2011) and may be written for end-members as follows:

$$\begin{aligned}&15CaCO_3\,(\text{aragonite}) + 6NaAlSi_2O_6\,(\text{jadeite})\\&\rightarrow 3Na_2Ca_4\,(CO_3)_5 + Ca_3Al_2Si_3O_{12}\,(\text{Ca-garnet}) +\\&2Al_2O_3\,(\text{corundum}) + 9SiO_2\,(\text{stishovite}).\end{aligned} \quad (13.1)$$

In the case of carbonated eclogite, where magnesite is the only carbonate entering the mantle transition zone, the corresponding reaction, taking place between 15 and 20 GPa (Thomson et al., 2016) should be written in a different way:

$$\begin{aligned}&15\,MgCO_3\,(\text{magnesite}) + 6\,NaAlSi_2O_6\,(\text{jadeite})\\&+4\,Ca_3Al_2Si_3O_{12}\,(\text{Ca-garnet}) \rightarrow 3\,Na_2Ca_4\,(CO_3)_5\\&+5\,Mg_3Al_2Si_3O_{12}\,(\text{Mg-garnet}) + 2\,Al_2O_3\,(\text{corundum})\\&+9\,SiO_2\,(\text{stishovite}).\end{aligned} \quad (13.2)$$

The latter reaction demonstrates an interesting ability of carbonates to extract not only sodium but also calcium from coexisting silicates at pressures of the mantle transition zone. Partitioning of calcium into Na-Ca carbonate also leads to the disappearance of aragonite from the subsolidus assemblage of carbonated pelite (and, in general, any Na-containing silicate lithology). The latter suggests that the only reliable solid-state hosts of oxidized carbon in the lower part of the mantle transition zone are Na-Ca carbonate and/or magnesite. Although the data of Grassi and Schmidt (2011) and Thomson et al. (2016) suggest that cold subduction geotherms pass well below the solidi of carbonated pelite and eclogite down to 660 km discontinuity, the possibility of carbonates transport from the mantle transition zone to the lower mantle requires additional studies.

13.4. CRYSTAL CHEMISTRY OF HIGH-PRESSURE NA-CA CARBONATES

In contrast to carbonates of calcium, magnesium, and iron, extensively studied during the last decade up to megabar pressures both theoretically and experimentally, the high-pressure chemistry of Na-Ca carbonates that hosts oxidized carbon in the mantle transition zone remains terra incognita.

The first systematic study of the Na_2CO_3-$CaCO_3$ system was done by Cooper et al. (1975) who reported its phase diagram at 1 kbar with two orthorhombic intermediate compounds: $Na_2Ca(CO_3)_2$ and $Na_2Ca_2(CO_3)_3$. Both of these compounds exist in natural forms, known as nyerereite and shortite minerals, respectively, although natural nyerereite always contains certain admixture of potassium, causing incommensurate modulation of its structure (Bolotina et al., 2017). Recently Song et al. (2017) reported hydrothermal synthesis at 220 °C of another intermediate compound, $Na_6Ca_5(CO_3)_8$, probably stable in the low-temperature field of Na_2CO_3-$CaCO_3$ phase diagram.

Room-temperature high-pressure behavior of nyerereite and shortite was recently studied by in situ Raman spectroscopy and X-ray diffraction (Borodina et al., 2018; Rashchenko, Goryainov, et al., 2017; Vennari et al., 2018). The equilibrium high-pressure investigation of the Na_2CO_3-$CaCO_3$ system was initiated by studies of its phase diagram at 3 and 6 GPa (Podborodnikov et al., 2018; Shatskiy et al., 2013, 2015; Litasov et al., this volume). The chemistry of intermediate Na-Ca carbonates turned out to be very sensitive to pressure (Figure 13.1): upon pressure increase from 0.1 to 3 GPa, the $Na_2Ca_2(CO_3)_3$ phase becomes unstable, while a new high-pressure $Na_2Ca_3(CO_3)_4$ phase appears on the phase diagram. A further pressure increase to 6 GPa leads to even more drastic changes: disappearance of $Na_2Ca(CO_3)_2$

and emergence of two new high-pressure phases, $Na_4Ca(CO_3)_3$ and $Na_2Ca_4(CO_3)_5$ on the phase diagram.

$Na_2Ca_3(CO_3)_4$. The crystal structure of $Na_2Ca_3(CO_3)_4$, stable at least between 3 and 6 GPa, was reported by Gavryushkin et al. (2014). The low symmetry (monoclinic) and long unit cell (a = 31.4421 Å, Table 13.2) of the compound are compensated by its strong pseudosymmetry, which allows reliable description of the structure using an orthorhombic cell with halved a parameter. Since the common approach of using cation-centered anion polyhedra could not provide a reliable structure description, Gavryushkin et al. proposed an alternative description based on stacking of cationic nets perpendicular to the a axis, with $(CO_3)^{2-}$ anions filling large cationic voids between adjacent nets. In the structure of $Na_2Ca_3(CO_3)_4$, cationic nets form two types of anion-filled layers, denoted A and B in Figure 13.2. In the A-type layers, $(CO_3)^{2-}$ anions are parallel to the a axis, whereas in the B-type layers they are oblique. The cationic voids hosting $(CO_3)^{2-}$ anions have the same geometry in both types of layers, namely a two-capped trigonal prism (Figure 13.3a). The Raman spectrum of the $Na_2Ca_3(CO_3)_4$ (Figures 13.4, 13.5c) is characterized by splitting of ν_4, ν_1, and $2\nu_2$ $(CO_3)^{2-}$ bands into up to three components due to the presence of several symmetrically independent carbonate anions in the structure.

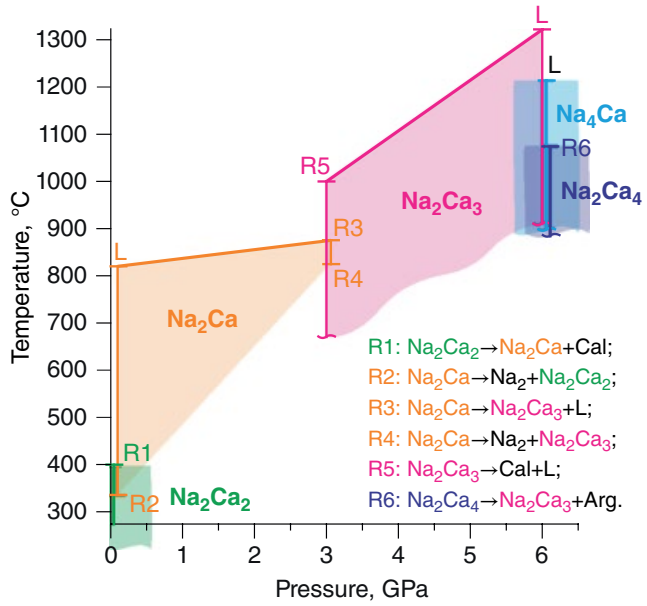

Figure 13.1 Variety of Na-Ca double carbonates established in the system Na_2CO_3–$CaCO_3$ at 0.1 GPa (Cooper et al., 1975), at 3 GPa (Podborodnikov et al., 2018), and at 6 GPa (Shatskiy et al., 2013). Na_2 = Na_2CO_3, Na_4Ca = $Na_4Ca(CO_3)_3$, Na_2Ca = $Na_2Ca(CO_3)_2$, Na_2Ca_2 = $Na_2Ca_2(CO_3)_3$, Na_2Ca_3 = $Na_2Ca_3(CO_3)_4$, Na_2Ca_4 = $Na_2Ca_4(CO_3)_5$, Arg = aragonite, Cal = calcite, L = carbonate melt. See electronic version for color representation of the figures in this book.

$Na_4Ca(CO_3)_3$. The crystal structure of $Na_4Ca(CO_3)_3$, stable at least at 6 GPa, was reported by Rashchenko et al. (2018). Rather unusual for carbonates, it has a cubic *Ia*–3*d* space group and can be described in a very elegant way using the same approach of cationic sublattice with anion-filled cavities. The cationic sublattice is represented by primitive cubic lattice with period of 0.25·a, where 25% of cubic voids are centered by Na^+ anions, and the remaining 75% are filled by $(CO_3)^{2-}$ anions (Figure 13.2). The resulting coordination of $(CO_3)^{2-}$ anion is a two-capped cube (Figure 13.3b). Although there is only one $(CO_3)^{2-}$ site in the structure, the Raman spectrum of the $Na_4Ca(CO_3)_3$

Table 13.2 Known Na-Ca carbonates (high-pressure phases are given in bold).

Formula and Synthesis Conditions	Space Group	Unit Cell, Å	Natural Analogue	Reference
$Na_2Ca(CO_3)_2$ 0.1 GPa/450 °C	$P2_1ca$ Z = 8	a = 10.0713(5) b = 8.7220(2) c = 12.2460(4)	*nyerereite* *$(Na,K)_2Ca(CO_3)_2$*	(Gavryushkin et al., 2016)
$Na_2Ca_2(CO_3)_3$ 220 °C (hydrothermal)	*Amm*2 Z = 2	a = 4.9720(9) b = 11.068(3) c = 7.1271(14)	*shortite* *$Na_2Ca_2(CO_3)_3$*	(Song et al., 2017)
$Na_6Ca_5(CO_3)_8$ 220 °C (hydrothermal)	$P6_3mc$ Z = 2	a = 10.0708(19) c = 12.604(4)	–	(Song et al., 2017)
$Na_2Ca_3(CO_3)_4$ 6 GPa/1400 °C	$P1n1$ Z = 8	a = 31.4421(8) b = 8.1960(2) c = 7.4360(2) β = 89.923(2)	–	(Gavryushkin et al., 2014)
$Na_4Ca(CO_3)_3$ 6 GPa/1200 °C	*Ia*–3*d* Z = 16	a = 14.5770(5)	–	(Rashchenko et al., 2018)
$Na_2Ca_4(CO_3)_5$ 6 GPa/1050 °C	$P6_3mc$ Z = 2	a = 10.37402(14) c = 6.25935(9)	*calcioburbankite* *$(Na,Ca,REE)_3(Ca,REE,Sr)_3(CO_3)_5$*	(Rashchenko, Bakakin, et al., 2017)

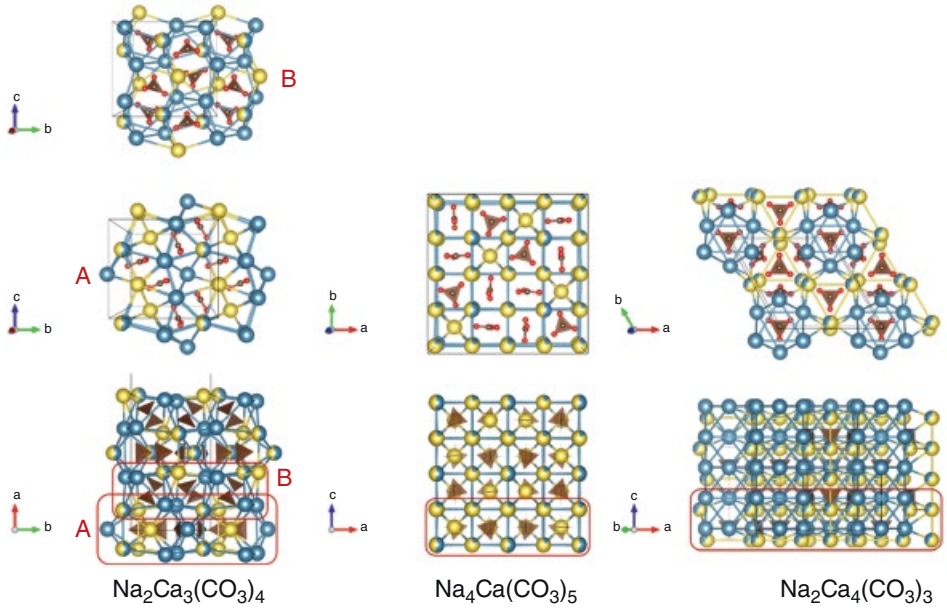

Figure 13.2 Crystal structures of high-pressure Na-Ca carbonates. Cationic layers filled with anions are shown in the top rows; overall view of structures with outlined layers is in the bottom one. Na^+ and Ca^{2+} cations are shown as yellow and blue, respectively; combined colors correspond to mixed sites. The drawing was prepared using VESTA software (Momma & Izumi, 2011). See electronic version for color representation of the figures in this book.

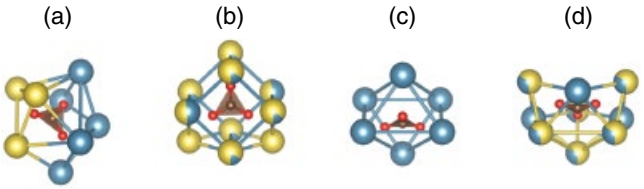

Figure 13.3 $(CO_3)^{2-}$ filled voids in cationic sublattice of high-pressure Na-Ca carbonates: (a) two-capped trigonal prism ($Na_2Ca_3(CO_3)_4$ and $Na_2Ca_4(CO_3)_5$), (b) two-capped cube ($Na_4Ca(CO_3)_5$), (c) octahedron ($Na_2Ca_4(CO_3)_5$), (d) three-capped trigonal prism ($Na_2Ca_4(CO_3)_5$). Na^+ and Ca^{2+} cations are shown as yellow and blue, respectively; combined colors correspond to mixed sites. See electronic version for color representation of the figures in this book.

exhibits clear splitting of ν_4, ν_1, and $2\nu_2$ $(CO_3)^{2-}$ bands (Figures 13.4, 13.5b), which can be explained by the lower (C_{2v}) local symmetry of the $(CO_3)^{2-}$ site.

$Na_2Ca_4(CO_3)_5$. The most interesting high-pressure Na-Ca carbonate is hexagonal ($P6_3mc$) $Na_2Ca_4(CO_3)_5$, synthesized at 6 GPa and strongly resembling the $(Na,K)_2(Ca,Mg,Fe)_4(CO_3)_5$ stoichiometry stable in carbonated pelite and eclogite under mantle transition zone conditions (Litasov et al., 2013; Thomson et al., 2016) (Table 13.1). Its crystal structure, reported by Rashchenko, Bakakin, et al., (2017), is also based on cationic nets perpendicular to the *c* axis (Figure 13.2), and contains three types of voids: two-capped trigonal prisms, also typical for $Na_2Ca_3(CO_3)_4$ (Figure 13.3a), octahedra (Figure 13.3c), and three-capped trigonal prisms (Figure 13.3d). The abundance of differently coordinated carbonate anions in the structure leads to the pronounced splitting of ν_4, ν_1, and $2\nu_2$ $(CO_3)^{2-}$ Raman bands into up to four components (Figures 13.4, 13.5a).

Importantly, among all reported high-pressure Na-Ca carbonates, the $Na_2Ca_4(CO_3)_5$ is the only one that has a natural analogue, *calcioburbankite* mineral, $(Na,Ca,REE)_3(Ca,REE,Sr)_3(CO_3)_5$ (Belovitskaya & Pekov, 2004). The apparent difference in formulae disappears if one rewrites the chemical $Na_2Ca_4(CO_3)_5$ formula into a structural $^{M1}(Na_2Ca)^{M2}Ca_3(CO_3)_5$ one, considering that the M1 cation site is occupied by $\frac{2}{3}Na^+$ and $\frac{1}{3}Ca^{2+}$, whereas M2 one is occupied solely by Ca^{2+} (Figure 13.2). A heterovalent $2Ca^{2+} \leftrightarrow Na^+ + REE^{3+}$ substitution herewith leads to *REE*-rich compositions, corresponding to natural calcioburbankites. Such a substitution (as well as incorporation of large Sr^{2+} and Ba^{2+} cations) very efficiently stabilizes the resulting structures at moderate pressures, so that natural calcioburbankites occur in carbonatites and alkali-rich pegmatites far from gigapascal pressures. A possibility of $Na_2Ca_4(CO_3)_5$ structure to incorporate large cations may have very important geochemical implications in the case of existence of this phase in the mantle transition zone. In contrast to $CaCO_3$ and $MgCO_3$ with limited capability to host REE and LILE, the appearance of the Na-Ca carbonate in equilibria with silicates will strongly deplete them in REE and LILE, leading to new patterns of trace element partitioning in the Earth's mantle.

An important crystal-chemical feature that unites all these high-pressure Na-Ca carbonates is their relation to

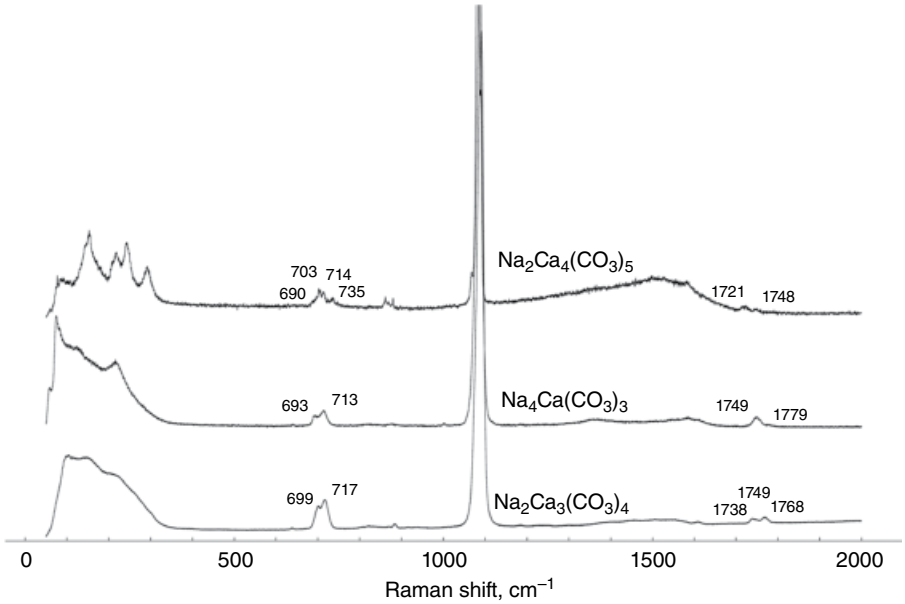

Figure 13.4 Raman spectra of high-pressure Na-Ca carbonates (deconvolutions of the main ν_1 $(CO_3)^{2-}$ band into individual components are shown in Figure 13.5). See electronic version for color representation of the figures in this book.

isostructural *borates*. Although crystal structures of ambient pressure Na-Ca carbonates have nothing in common with the latter class of compounds, their high-pressure counterparts adopt exactly the same crystal structures that were described years ago for borate materials (Table 13.3). Another crystal-chemical feature of high-pressure Na-Ca carbonates is a presence of mixed Na-Ca sites in their crystal structures (Figure 13.2), unusual for nyerereite and shortite.

Besides the high-pressure Na-Ca carbonates discussed above, we should mention the following:

1. In two subsolidus experiments (at 22 GPa/1350 °C and 23.5 GPa/1400 °C) Grassi and Schmidt (2011) also reported the existence of nearly pure $Na_2Ca_2(CO_3)_3$ phase together with $(Na,K)_2(Ca,Mg,Fe)_4(CO_3)_5$ discussed above, in the carbonated pelite.

2. In a subsolidus experiment at 21 GPa/1200 °C, Kiseeva et al. (2013) reported $(Na,K)_2(Ca,Mg,Fe)(CO_3)_2$ phase coexisting with "Na-aragonite" (Na-Ca carbonate with Na_2O up to 8 wt.%) in a carbonated eclogite. A similar assemblage was reported by Litasov et al. (2013) for subsolidus conditions of Na-bearing carbonatite composition at 15.5 GPa and 1100 °C. Unfortunately, only the chemical composition was reported for Na-Ca carbonates in all listed studies.

Although at ambient pressure $Na_2Ca_2(CO_3)_3$ and $Na_2Ca(CO_3)_2$ stoichiometries correspond to shortite and nyerereite, which decompose below 3 and 6 GPa, respectively, one cannot exclude that high-pressure polymorphs of these minerals may exist at pressures of the mantle transition zone. "Na-aragonite" may represent an unknown Ca-rich high-pressure Na-Ca carbonate, because no evidence of sodium incorporation into aragonite was reported by Shatskiy et al. (2013) or Podborodnikov et al. (2018), at least up to 6 GPa. On the other hand, taking into account a known problem of Na_2O underestimation in carbonates by WDS and EDS (Shatskiy et al., 2013), one can suggest that real Na_2O content of "Na-aragonite" may exceed 10 wt.%, actually corresponding to the discussed $(Na,K)_2(Ca,Mg,Fe)_4(CO_3)_5$ phase.

13.5. CONCLUSIONS

High-pressure experiments in the carbonate-silicate systems replicating eclogite (Kiseeva et al., 2013; Thomson et al., 2016), pelite (Grassi & Schmidt, 2011), and model carbonatite (Litasov et al., 2013) revealed a number of Na-Ca carbonates resembling stoichiometries of $Na_2Ca(CO_3)_2$ nyerereite, $Na_2Ca_2(CO_3)_3$ shortite, and $Na_2Ca_4(CO_3)_5$ burbankite. Stabilization of these carbonates within oceanic crust subducted to the mantle transition zone can decrease drastically the solidus temperatures and cause formation of sodic dolomitic carbonatite melts.

Considering the phase relations in the Na_2CO_3–$CaCO_3$ system (Cooper et al., 1975; Podborodnikov et al., 2018; Shatskiy et al., 2013, 2015), a range of Na-Ca double carbonates changes in the following sequence upon pressure and temperature increase: $Na_2Ca(CO_3)_2$, $Na_2Ca_2(CO_3)_3$, (0.1 GPa) → $Na_2Ca(CO_3)_2$, $Na_2Ca_3(CO_3)_4$ (3 GPa) → $Na_4Ca(CO_3)_3$, $Na_2Ca_3(CO_3)_4$,

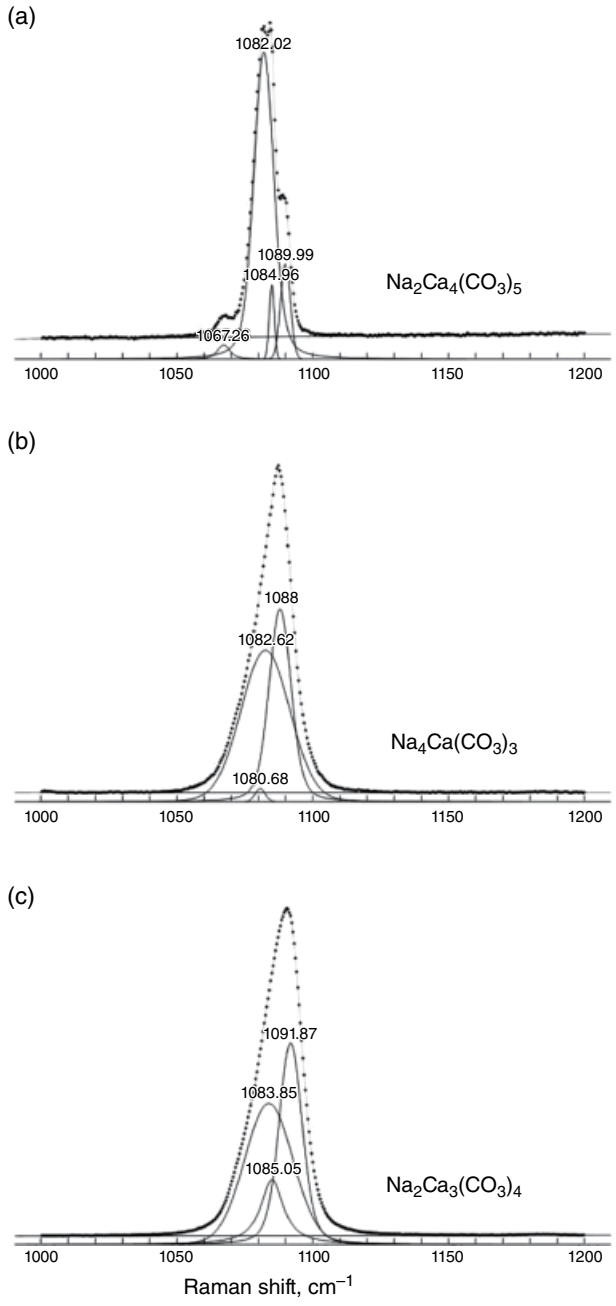

Figure 13.5 Deconvolutions of the main ν_1 $(CO_3)^{2-}$ band into individual components for the Raman spectra of high-pressure Na-Ca carbonates. See electronic version for color representation of the figures in this book.

$Na_2Ca_4(CO_3)_5$ (6 GPa). The Na-Ca carbonates recovered from experiments at 0.1, 3, and 6 GPa were characterized by Raman spectroscopy and their crystal structures were solved: $Na_4Ca(CO_3)_3$ (*Ia*−3*d*) (Rashchenko et al., 2018), $Na_2Ca(CO_3)_2$ ($P2_1ca$) nyerereite (Gavryushkin et al., 2016), $Na_2Ca_3(CO_3)_4$ (P1n1) (Gavryushkin et al., 2014; Shatskiy et al., 2015), $Na_2Ca_4(CO_3)_5$ ($P6_3mc$) burbankite (Rashchenko, Bakakin, et al., 2017).

Table 13.3 Borate analogs of high-pressure Na-Ca carbonates.

High-Pressure Na-Ca Carbonates	Space Group	Ambient-Pressure Borates	Reference
$Na_2Ca_3(CO_3)_4$ a = 7.4360 Å b = 15.72 Å c = 8.1960 Å	*Pnma**	$Nd_2Ba_3(BO_3)_4$ a = 7.7143(11) Å b = 16.7790(34) Å c = 8.9478(14) Å	(Yan & Hong, 1987)
$Na_4Ca(CO_3)_3$ a = 14.5770(5) Å	*Ia–3d*	$NaBa_4(BO_3)_3$ a = 15.783(4) Å	(Kokh et al., 2004)
$Na_2Ca_4(CO_3)_5$ a = 10.37402(14) Å c = 6.25935(9) Å	$P6_3mc$	$Ca_3La_3(BO_3)_5$ a = 10.530(3) Å c = 6.398(2) Å	(Zhou & Ye, 2008)

* Pseudosymmetry for $Na_2Ca_3(CO_3)_4$.

Although in situ high-pressure studies of Na-Ca carbonates have just begun (Borodina et al., 2018; Vennari et al., 2018), they already suggest an existence of unquenchable high-pressure polymorphs of $Na_2Ca_2(CO_3)_3$ and probably $Na_2Ca(CO_3)_2$ at pressures exceeding 15 GPa. The compounds with similar stoichiometries were also observed in quench experiments. Grassi and Schmidt (2011) detected carbonate resembling shortite composition at 22 and 23.5 GPa in carbonated pelite, whereas Kiseeva et al. (2013) found carbonate resembling nyerereite stoichiometry at 21 GPa in carbonated eclogite. Both compounds were observed in subsolidus assemblages of model Na-bearing carbonatite (Litasov et al., 2013).

ACKNOWLEDGMENTS

The work was supported by the Russian Science Foundation (No 14-17-00609-P) and performed under the Deep Carbon Observatory program.

REFERENCES

Belovitskaya, Y. V., & Pekov, I. V. (2004). Genetic mineralogy of the burbankite group. *New Data on Minerals*, *39*, 50–64.

Bolotina, N. B., Gavryushkin, P. N., Korsakov, A. V., Rashchenko, S. V., Seryotkin, Y. V., Golovin, A. V., et al. (2017). Incommensurately modulated twin structure of nyerereite $Na_{1.64}K_{0.36}Ca(CO_3)_2$. *Acta Crystallographica B*, *73*, 276–284.

Borodina, U., Likhacheva, A., Golovin, A., Goryainov, S., Rashchenko, S., & Korsakov, A. (2018). Raman spectra of shortite $Na_2Ca_2(CO_3)_3$ compressed up to 8 GPa. *High Pressure Research*, *38*, 293–302.

Brovarone, A. V., Martinez, I., Elmaleh, A., Compagnoni, R., Chaduteau, C., Ferraris, C., & Esteve, I. (2017). Massive

production of abiotic methane during subduction evidenced in metamorphosed ophicarbonates from the Italian Alps. *Nature Communications*, *8*, 14134.

Cooper, A. F., Gittins, J., & Tuttle, O. F. (1975). The system Na_2CO_3-K_2CO_3-$CaCO_3$ at 1 kilobar and its significance in carbonatite petrogenesis. *American Journal of Science*, *275*, 534–560.

Debret, B., Bolfan-Casanova, N., Padrón-Navarta, J. A., Martin-Hernandez, F., Andreani, M., Garrido, C. J., et al. (2015). Redox state of iron during high-pressure serpentinite dehydration. *Contributions to Mineralogy and Petrology*, *169*, 313.

Faccenda, M. (2014). Water in the slab: A trilogy. *Tectonophysics*, *614*, 1–30.

Gavryushkin, P. N., Bakakin, V. V., Bolotina, N. B., Shatskiy, A. F., Seryotkin, Y. V., & Litasov, K. D. (2014). Synthesis and crystal structure of new carbonate $Ca_3Na_2(CO_3)_4$ homeotypic with orthoborates $M_3Ln_2(BO_3)_4$ (M = Ca, Sr, and Ba). *Crystal Growth & Design*, *14*, 4610–4616.

Gavryushkin, P. N., Martirosyan, N. S., Inerbaev, T. M., Popov, Z. I., Rashchenko, S. V., Likhacheva, A. Y., et al. (2017). Aragonite-II and $CaCO_3$-VII: New high-pressure, high-temperature polymorphs of $CaCO_3$. *Crystal Growth & Design*, *17*, 6291–6296.

Gavryushkin, P. N., Thomas, V. G., Bolotina, N. B., Bakakin, V. V., Golovin, A. V., Seryotkin, Y. V., et al. (2016). Hydrothermal synthesis and structure solution of $Na_2Ca(CO_3)_2$: "Synthetic analogue" of mineral nyerereite. *Crystal Growth & Design*, *16*, 1893–1902.

Grassi, D., & Schmidt, M. W. (2011). The melting of carbonated pelites from 70 to 700 km depth. *Journal of Petrology*, *52*, 765–789.

Hammouda, T., & Keshav, S. (2015). Melting in the mantle in the presence of carbon: Review of experiments and discussion on the origin of carbonatites. *Chemical Geology*, *418*, 171–188.

Kaminsky, F. V. (2017). *The Earth's lower mantle: Composition and structure*. New York: Springer.

Kerrick, D. M., & Connolly, J.A.D. (2001). Metamorphic devolatilization of subducted oceanic metabasalts: Implications for seismicity, arc magmatism and volatile recycling. *Earth and Planetary Science Letters*, *189*, 19–29.

Kiseeva, E. S., Litasov, K. D., Yaxley, G. M., Ohtani, E., & Kamenetsky, V. S. (2013). Melting and phase relations of carbonated eclogite at 9–21 GPa and the petrogenesis of alkali-rich melts in the deep mantle. *Journal of Petrology*, *54*, 1555–1583.

Kiseeva, E. S., Vasiukov, D. M., Wood, B. J., McCammon, C., Stachel, T., Bykov, M., et al. (2018). Oxidized iron in garnets from the mantle transition zone. *Nature Geoscience*, *11*, 144–147.

Kodolányi, J., Pettke, T., Spandler, C., Kamber, B. S., & Gméling, K. (2011). Geochemistry of ocean floor and fore-arc serpentinites: Constraints on the ultramafic input to subduction zones. *Journal of Petrology*, *53*, 235–270.

Kokh, A. E., Kononova, N. G., Bekker, T. B., Furmanova, N. G., Maximov, B. A., Bolotina, N. B., et al. (2004). New sodium barium orthoborate $NaBa_4(BO_3)_3$. *Russian Journal of Inorganic Chemistry*, *49*, 984–988.

Korenaga, J. (2017). On the extent of mantle hydration caused by plate bending. *Earth and Planetary Science Letters*, *457*, 1–9.

Litasov, K. D. (2011). Physicochemical conditions for melting in the Earth's mantle containing a C–O–H fluid (from experimental data). *Russian Geology and Geophysics*, *51*, 475–492.

Litasov, K. D., & Shatskiy, A. (2018). Carbon-bearing magmas in the Earth's deep interior. In Y. Kono & C. Sanloup (Eds.), *Magmas Under Pressure* (pp. 43–82). Amsterdam: Elsevier.

Litasov, K. D., Shatskiy, A., Ohtani, E., & Yaxley, G. M. (2013). Solidus of alkaline carbonatite in the deep mantle. *Geology*, *41*, 79–82.

Luth, R.W. (2001). Experimental determination of the reaction aragonite plus magnesite = dolomite at 5 to 9 GPa. *Contributions to Mineralogy and Petrology, 141*, 222−232.

Merlini, M., Cerantola, V., Gatta, G. D., Gemmi, M., Hanfland, M., Kupenko, I., et al. (2017). Dolomite-IV: Candidate structure for a carbonate in the Earth's lower mantle. *American Mineralogist*, *102*, 1763–1766.

Momma, K., & Izumi, F. (2011). VESTA 3 for three-dimensional visualization of crystal, volumetric and morphology data. *Journal of Applied Crystallography*, *44*, 1272–1276.

Oganov, A. R., Ono, S., Ma, Y. M., Glass, C. W., & Garcia, A. (2008). Novel high-pressure structures of $MgCO_3$, $CaCO_3$ and CO_2 and their role in Earth's lower mantle. *Earth and Planetary Science Letters*, *273*, 38–47.

Pickard, C. J., & Needs, R. J. (2015). Structures and stability of calcium and magnesium carbonates at mantle pressures. *Physical Review B*, *91*, 104101.

Plank, T., & Langmuir, C. H. (1998). The chemical composition of subducting sediment and its consequences for the crust and mantle. *Chemical Geology*, *145*, 325–394.

Podborodnikov, I. V., Shatskiy, A., Arefiev, A. V., Rashchenko, S. V., Chanyshev, A. D., & K. D. Litasov (2018). The system Na_2CO_3–$CaCO_3$ at 3 GPa. *Physics and Chemistry of Minerals*, *45*, 773–787.

Rashchenko, S. V., Bakakin, V. V., Shatskiy, A. F., Gavryushkin, P. N., Seryotkin, Y. V., & Litasov K. D. (2017). Noncentrosymmetric $Na_2Ca_4(CO_3)_5$ carbonate of "$M1_3M2_3XY_3Z$" structural type and affinity between borate and carbonate structures for design of new optical materials. *Crystal Growth & Design*, *17*, 6079–6084.

Rashchenko, S. V., Goryainov, S. V., Romanenko, A. V., Golovin, A. V., Korsakov, A. V., Moine, B. N., & Mikhno A. O. (2017). High-pressure Raman study of nyerereite from Oldoinyo Lengai. *Journal of Raman Spectroscopy*, *48*, 1438–1442.

Rashchenko, S., Shatskiy, A., Arefiev, A., Seryotkin Y., & Litasov, K. (2018). $Na_4Ca(CO_3)_3$: A novel carbonate analog of borate optical materials, *CrystEngComm*, *20*, 5228–5232,.

Sato, K., & Katsura, T. (2001). Experimental investigation on dolomite dissociation into aragonite+magnesite up to 8.5 GPa. *Earth and Planetary Science Letters*, *184*, 529–534.

Shatskiy, A., Gavryushkin, P. N., Litasov, K. D., Koroleva, O. N., Kupriyanov, I. N., Borzdov, Y. M., et al. (2015). Na-Ca carbonates synthesized under upper-mantle conditions: Raman spectroscopic and X-ray diffraction studies. *European Journal of Mineralogy*, *27*, 175–184.

Shatskiy, A., Sharygin, I. S., Litasov, K. D., Borzdov, Y. M., Palyanov, Y. N., & Ohtani, E. (2013). New experimental data on phase relations for the system Na_2CO_3-$CaCO_3$ at 6 GPa and 900-1400 °C. *American Mineralogist*, *98*, 2164–2171.

Shilobreeva, S., Martinez, I., Busigny, V., Agrinier, P., & Laverne, C. (2011). Insights into C and H storage in the altered oceanic crust: Results from ODP/IODP Hole 1256D. *Geochimica et Cosmochimica Acta*, *75*, 2237–2255.

Song, Y., Luo, M., Zhao, D., Peng, G., Lin, C., & Ye, N. (2017). Explorations of new UV nonlinear optical materials in the Na_2CO_3–$CaCO_3$ system. *Journal of Materials Chemistry C*, *5*, 8758–8764.

Stagno, V. (2019). Carbon, carbides, carbonates and carbonatitic melts in the Earth's interior. *Journal of Geological Society*, doi.org/10.1144/jgs2018-1095 (in press).

Stagno, V., Frost, D., McCammon, C., Mohseni, H., & Fei, Y. (2015). The oxygen fugacity at which graphite or diamond forms from carbonate-bearing melts in eclogitic rocks. *Contributions to Mineralogy and Petrology*, *169*(2), 1–18.

Staudigel, H. (2014). Chemical fluxes from hydrothermal alteration of the oceanic crust. In K. K. Turekian & H. D. Holland (Eds.), *Treatise on Geochemistry* (2nd ed., pp. 583–606) Oxford: Elsevier.

Thomson, A. R., Walter, M. J., Kohn, S. C., & Brooker, R. A. (2016). Slab melting as a barrier to deep carbon subduction. *Nature*, *529*, 76–79.

Vennari, C. E., Beavers, C. M., & Williams, Q. (2018). High-pressure/temperature behavior of the alkali/calcium carbonate shortite ($Na_2Ca_2(CO_3)_3$): Implications for carbon sequestration in Earth's transition zone. *Journal of Geophysical Research: Solid Earth*, *123*, 6574–6591.

Yan, J. F., & Hong, H.Y.-P. (1987). Crystal structure of a new mini-laser material. $Nd_2Ba_3(BO_3)_4$. *Materials Research Bulletin*, *22*, 1347–1353.

Zhou, T., & Ye, N. (2008). Redetermination of tricalcium trilanthanum pentakis (orthoborate) from single-crystal data. *Acta Crystallographica E*, *64*, i37.